Near surface austenite grain growth in different casting processes for steel: Experiments and modeling

Christian Bernhard, Sergey Bragin, Wolfgang Vanovsek
Montanuniversitaet Leoben, Leoben, Austria
Corresponding author: e-mail christian.bernhard@unileoben.ac.at

The present paper focuses on the experimental and numerical characteristics of near surface austenite grain growth in the continuous casting of slabs, thin slabs and strips. The paper focuses on the metallographic analysis of different solidification experiments at higher cooling rates. This comprises particularly dipping experiments but also the in-situ observation of austenite grain growth by high-temperature laser scanning confocal microscopy (LSCM). The results were utilized to adjust model parameters like the composition dependency of the activation energy for grain growth. The results of the model are finally compared with selected results of the austenite grain size measurement on slab, thin slab and cast strip samples.

Key words: Continuous casting, austenite grain growth, precipitation

Introduction

In the continuous casting of slabs, blooms and billets, coarse austenite grains may raise the risk of the formation of surface cracks. In thin slab casting and direct rolling (TSCR) the austenite grain size after casting, or after homogenisation of temperature respectively, is an important initial parameter for dynamic recrystallisation in the rolling process. In thin strip casting (TSC), the austenite grain size is of highest relevance for the microstructure evolution and thus for the mechanical properties of the final product.
The growth of austenite grains during cooling after solidification is mainly influenced by the steel composition and the cooling rate. In rolling processes, the pinning forces caused by precipitations are most important for austenite grain growth, too. In contrast, the short residence time of the surface at elevated temperature in TSC and TSCR prevents the formation of precipitations along grain boundaries in a sufficient volume fraction to retard the growth of austenite grains.
The formation of transverse surface cracks has been a vital topic for several decades and the importance of coarse austenite grains was already recognized at an early stage [1-3]. Based on the differentiation between a first and second brittle temperature range for steels at elevated temperature, the formation of transverse cracks is commonly attributed to an overcritical deformation in the second ductility trough. The second ductility trough is caused by the formation of precipitates, phases or segregates along austenite grain boundaries. Besides some alloying and micro-alloying elements also process related factors, like deep oscillation marks or surface depressions [4-6] on the strand surface, associated with coarse austenite grain size [7, 8] worsen the crack susceptibility.
Besides the notch effect and the associated stress concentration within the oscillation mark, the reduced heat transfer in this area will result in the formation of coarse austenite grains. An increasing austenite grain size has a remarkable influence on the ductility in the second ductility trough as the specific grain boundary area decreases while the precipitate density increases [9]. Cracks may also propagate easier by sliding fewer triple points [3] and the critical strain for the onset of dynamic recrystallization increases [10, 11]. According to Mintz et al. [3], the minimum RA in the second ductility trough is reciprocal to the square root of the austenite grain diameter with decreasing influence of grain diameters above 300 µm. Other authors, like Ohmori and Kunitake [12], found the elongation to be reciprocal to the grain diameter for grain diameters above 100 µm.

1. Numerical prediction of austenite grain growth

Since the fundamental work of Yasumoto et al. and Maehara et al. [4, 13, 14] the most important influencing parameters on the growth of austenite

grains during cooling of steel after solidification are well known: steel composition, the starting temperature for austenite grain growth and the cooling rate during and after solidification.
In a recent paper [15] the authors presented an austenite grain growth model for continuous casting based on the approach of Andersen and Grong [16] and fitted to own experimental results:

$$\frac{d\,\overline{D}}{dt} = M_0^{*} \cdot e^{-\frac{Qapp}{R \cdot T}} \cdot \left(\frac{1}{\overline{D}} - \frac{1}{k} \cdot q_p \right)^{\left(\frac{1}{n}-1\right)} \qquad (1)$$

In this formula M_0^{*} - assumed to be $4 \cdot 10^{-3}$ $m^2 s^{-1}$ [17] - denotes a kinetic constant that describes the grain boundary mobility in $m^2 s^{-1}$. Q_{app} is the apparent activation energy for grain growth in J/mol and R is the gas constant (8.3145 J/molK). T is the temperature in [K]. The driving force for grain growth is thus reciprocal to the actual grain diameter. This driving force is counteracted by a pinning force, exerted by precipitations on the grain boundaries. The term k/q_p represents the maximum grain diameter under normal grain growth conditions, the so-called Zener limit. According to the Zener model, K is assumed to be 4/3 [17]. $q_p(t)$ denotes the pinning force parameter, f the volume fraction of particles in a certain class and r the mean radius of the particles in this class.

$$q_p(t) = \frac{f}{r} = \int_0^t \frac{f(t,\tau)}{r(t,\tau)} d\tau \qquad (2)$$

The time exponent n was assumed to be 0.5.

Fig. 1. Measured (D_0, D_{10}) and calculated austenite grain size grain size D_{calc} close to the surface of slabs [15]

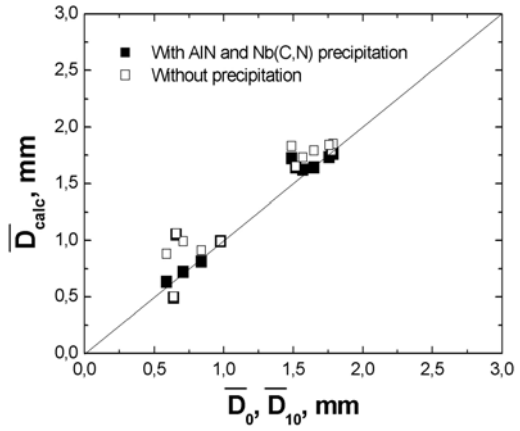

From laboratory solidification experiments, the following linear function for the dependency of the activation energy from the carbon content has been proposed:

$$Q_{app} = 167686 + 40562 \cdot (mass - \%C) \qquad (3)$$

Finally the results of the model were verified by metallographic examinations on slabs with between 0.15 mass-% and 0.53 mass-% carbon, Fig. 1.
This model has more recently been coupled with the inclusion kinetics of Matcalc [18,19] and extended to lower carbon content and higher cooling rates. The present paper focuses on the metallographic analysis of different solidification experiments at a higher cooling rate. This comprises particularly the well known dipping experiments but also the in-situ observation of austenite grain growth by high-temperature laser scanning confocal microscopy (LSCM).

2. Experimental work

In general, two types of experiments can be considered for the analysis of austenite grain growth:

- *Indirect methods* comprise isothermal or non-isothermal heat treatment and the subsequent measurement of the size of the former austenite grains by light microscopy or electron microscopy. If the experiment has to be relevant for casting processes, it is required to start the experiment with the solidification of the sample and the solidification conditions have to be adjusted to the simulated process [e.g. 4, 17]. The reason for this demand will be explained later on.
- *Direct methods* comprise methods for the direct observation of austenite grain growth. The most usual method – gaining growing importance in many actual publications – is high-temperature laser scanning confocal microscopy (HT-LSCM) [e.g. 20]. In the following section, some examples for HT-LSCM measurement will be quoted and the advantages of HT-LSCM will be discussed.

2.1 Indirect methods

For the aforementioned measurement of the former austenite grain size on samples from laboratory experiments [15], a dipping experiment - the so-called SSCT-experiment - was used without performing a tensile test. Details for the experimental parameters can be found in [15, 21]. Main objective of these experiments was to simulate the relatively moderate cooling rates during the solidification in the slab casting process. The cooling rate after emerging the solidified sample off the melt was high enough to prevent the precipitation of nitrides and carbonitrides and thus to eliminate pinning forces. A further increase of the cooling rate during the γ/α-transformation – a prerequisite to visualize the former austenite grains

in the metallographic examinations also for low carbon steel grades - proved to be impossible.
Therefore, a modified experimental setup was chosen, as depicted in Fig. 2. A steel tube filled with aluminium was submerged into a steel melt. During the experiment the heat withdrawal from the melt is mainly controlled by the latent heat of the aluminium core. After a certain solidification time, the shell is emerged and either held isothermal at a defined temperature in a chamber furnace for a given time and subsequently quenched in water sprays. Table 1 gives the composition of the tested steel grade.

Table 1. Steel composition for experiments

C, wt.-%	Si, wt.-%	Mn, wt.-%	Al, wt.-%
0.06	0.3	0.25	0.03

Fig. 3 shows the calculated temperatures in different distances from the surface and for varying holding time at 1100°C. The precipitation kinetic for AlN has been calculated with Matcalc [22]. The AlN-precipitates form not before the quenching of the sample, their influence on the austenite grain size is thus negligible.

Fig 2. Experimental simulation of austenite grain growth.

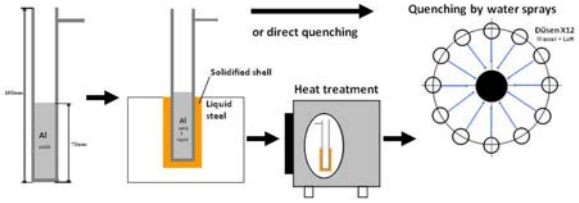

Fig 3. Calculated temperatures in different distances from the chill/shell interface and for varying holding time at 1100°C, kinetics of AlN-precipitation for 0.03 wt.-% Al and 0.008 wt.-%N.

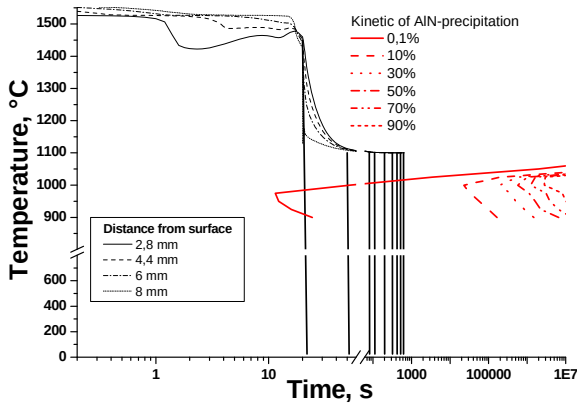

Fig 4. Micrographs for samples with different thermal history

Sample, quenched immediately after solidification	Sample, isothermal holding at 1100°C for 120s.
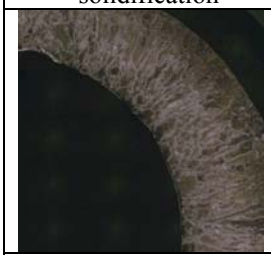	

Fig. 4 illustrates the importance of the directional solidification for the morphology of the austenite grains: On the left side – the sample was quenched immediately after solidification – the austenite grains appear in the majority columnar, very similar to cast semi finished products. The grain size is here determined by the measurement of intercepts, viz. the measurement of a large number of grain diameters and not the grain length. After isothermal holding at 1100°C for 120 s (right side), the grains appear polygonal shaped. This might - in the case of the present experiment and in contrast with the experimental results in [15] - be attributed to the relatively small thickness of the sample in relation to the grain size. The grain growth kinetic depends on the shape of the grains and should be different for columnar and polygonal grains.

Fig 5. Measured austenite grain size vs. holding time at 1100°C.

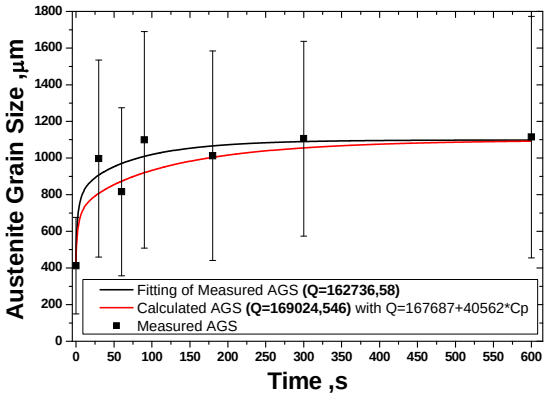

Fig. 5 summarizes the results for isothermal holding of the sample at 1100°C. The fitting of the experimental results by Equation 1 and the previously described input data, would result in the calculated activation energy of 162.736 J/mol. This comes close to the activation energy predicted from eq. (3), which is 169.024 J/mol for the steel composition in Table 1. Minor differences between the two solutions occur mainly during the first few hundred seconds. For a longer isothermal holding of the temperature, the predicted results from eq. (3) correspond very well with the measured grain size. For the prediction of austenite grain growth in

slab casting of steels with less than 0.1 wt.-% C (like typical HSLA and LC steels), these assumptions will thus lead to sufficiently reliable results.

The verification of these results by the comparison with the measured grain size on the slab surface was one original objective but appeared to be impossible by common metallographic techniques. Nevertheless, the results correspond very well with the measured former austenite grain size at continuously cast thin slabs, as will be shown later on.

As already explained in the introduction, coarse austenite grains are an important influencing factor for surface crack formation in slab casting. In thin slab casting and direct rolling, the austenite grain size is a decisive starting parameter for microstructure evolution in the rolling process. In strip casting and welding – assuming no further thermal or thermo-mechanical recrystallisation – fine austenite grains are a key factor for the achievement of excellent mechanical properties of the product.

The numerical simulation of grain growth for high cooling rates could thus be a further promising application for the here presented model. Basis is again the physical simulation of grain growth for rapid solidification processes.

The simulation experiment is based on the principle of a dipping test, as for example already realized by Mahapatra et al. in the 1990s [23,24,]. A substrate, made from a conventional mold copper alloy - coated with Cr or Ni and with controlled surface roughness - is submerged into a steel melt at high velocity, Fig. 6 [25]. The experiment is performed inside a vacuum induction furnace under inert gas. The rectangular substrate is surrounded by a non-wetting, insulating refractory brick that prevents the solidification of the steel. Thus, an 80 mm x 40 mm flat, rectangular sample solidifies at the surface of the substrate under conditions close to the simulated process. During the dwell time in the melt – typically ranging from 0.25 s to 3 s (depending on the simulated process) - the shrinkage of the thin sample induces friction forces between the sample and the substrate, which might result in the formation of microcracks. Investigations on the interaction between process parameters like surface roughness and steel composition on the one hand and the formation of microcracks on the other hand were the initial intention behind the development of this experiment. Later on, the experiment was adopted by the optical measurement of the sample temperature after emerging and the optional controlled cooling and heat treatment of the samples. This provides the opportunity to perform austenite grain growth experiments with relevance for strip casting and welding of steels.

Fig 6. Experimental procedure for dipping experiments with subsequent controlled cooling [25]

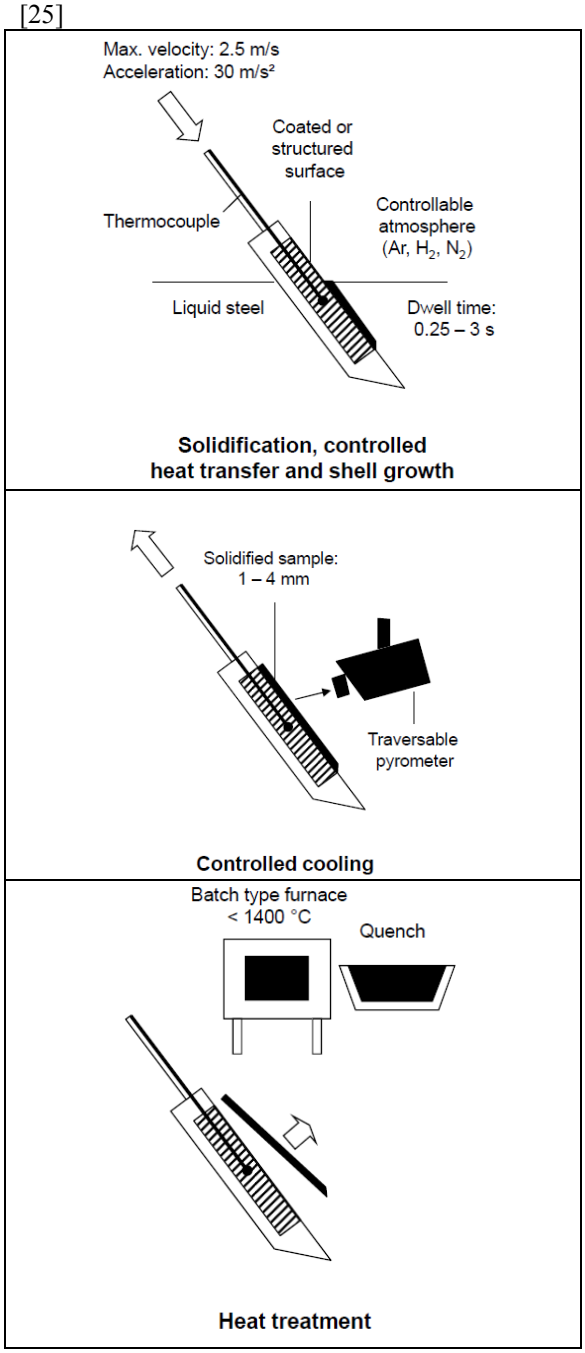

Fig. 7 illustrates the metallografic examination of the samples and depicts the measured grain size distribution after the solidification of a 0.06 wt.%-C steel grade, Table 2.

Table 2. Steel composition for results in Fig. 7 [26]

C, wt.-%	Si, wt.-%	Mn, wt.-%	Cr, wt.-%	Mo, wt.-%	Ni, wt.-%
0.06	0.7	1.5	0.4	0.3	2.0

Fig 7. Metallografic examination and measured austenite grain size (intercepts) for the steel grade in Table 2, 0.25 s solidification, cooling by radiation [26]

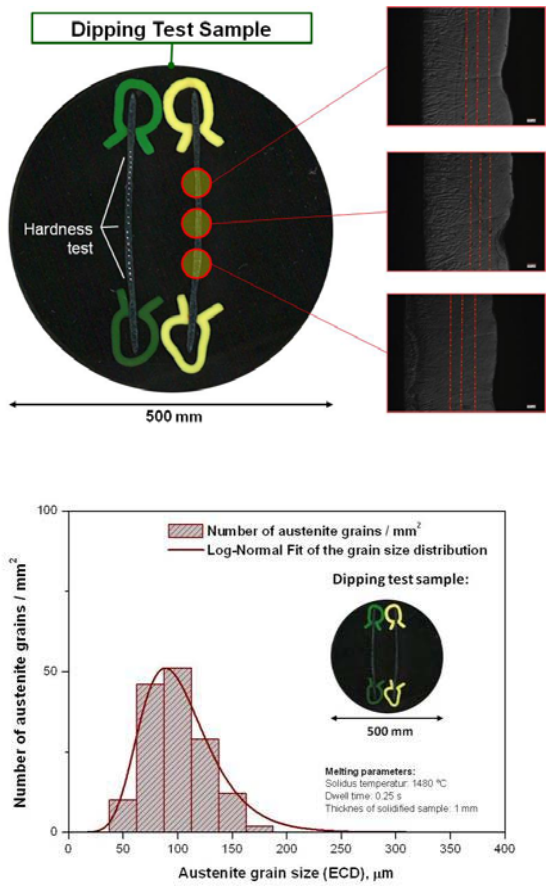

The maximum in the lognormal-distribution is 80 µm. This experiment is currently used to investigate the influence of alloying elements and precipitates on the austenite grain size, which by itself is a decisive factor for the formation and the refinement of acicular ferrite. Fig. 8 shows as an example the mean austenite grain size for the steel grade in table 2 versus the Ti-content in wt.-%. In Fig. 8, Ti turns out to have only a minor influence on the austenite grain size, but nevertheless, Ti influences the volume fraction of acicular ferrite in the sample after the experiment significantly.

Finally, Fig. 9 gives an example for the comparison of calculated and measured austenite grain size for the dipping experiment: The calculations seem to overestimate the austenite grain growth by appr. 20-30%. Two main reasons for the divergence can be named: inaccuracies in the calculated thermal history and the influence of Ni, Cr and Mo on the activation energy for grain growth. The model calculations are very sensitive for even small changes in cooling rates at temperatures close to the solidus temperature. However, the correspondence between measurement and calculation is evident and is sufficient for most applications.

Fig 8. Mean austenite grain size (ECD) for the steel grade in Table 2 versus Ti-content, 0.25 s solidification, cooling by radiation [26]

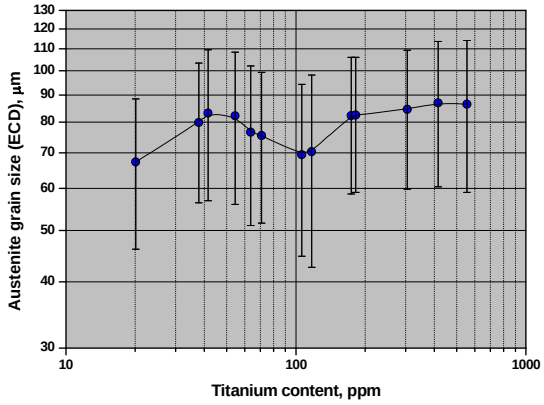

Fig 9. Austenite grain growth (ECD) for the steel grade in Table 2, 0.25 s solidification, cooling by radiation, calculated and measured

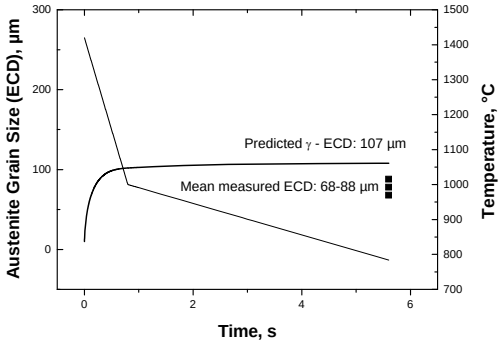

Fig 10. Austenite grain size (ECD) at 800 °C, constant cooling rate below T^{γ}, three different steel grades and indicated range of technical processes

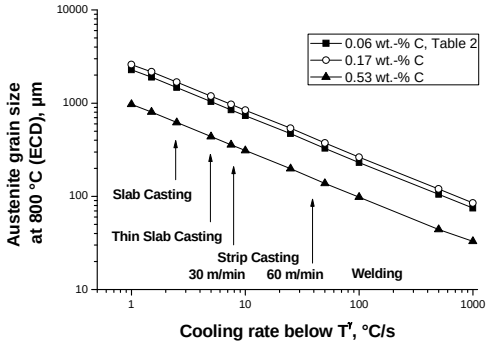

Fig. 10 summarizes the influence of cooling rate and steel composition in one diagram. The thermal boundary conditions were assumed as constant cooling rate below the T^{γ} temperature. The T^{γ} temperature was assumed with 1420 °C for the 0.06 wt.-% C steel, 1495 for the 0.17 wt.-% C steel and 1390 °C for the 0.53 wt.-% carbon steel. The largest austenite grains will be found for the 0.17 wt.-% C steel, the second largest for the 0.06 wt.-% C steel

and the finest grains for the 0.53 wt.-% carbon steel.

Cooling rates of 1.5 – 2.5 °C/s result in a typical austenite grain size of between 1.5 and 2.5 mm for the 0.06 and 0.17 wt.-% C steel grades. This is the typical size of former austenite grains close to the surface of slabs [15]. The austenite grain size *at* the surface of slabs is somewhat smaller and ranges between 0.7 and 1.2 mm, according to a cooling rate of 5 – 10 °C/s. It is worth noting that the cooling rate in casting process is not constant and usually higher at the beginning of solidification. The time for grain growth at elevated temperature is therefore lower. However, grain growth is a thermally activated process and thus much faster at higher temperatures. The rather small initial grain size is a further driving factor for grain growth. In addition of these influencing factors, the cooling rate during initial solidification (e.g. in the mold) is the dominating factor for the final austenite grain size, compare Fig. 9. The cooling rate for the simplified assumptions underlying Fig. 10 should – taking slab casting as an example - therefore be correlated with the cooling rates in the mold and *not* with the cooling rate in the secondary cooling zone.

In thin slab casting, the cooling rate at the surface in the mold is similar to slab casting but slightly higher. Measurement on thin slabs, cast at 6 m/min, point to a typical austenite grain size of between 0.4 and 0.7 mm [27] for steel grades with 0.06 and 0.17 wt.-% C.

In strip casting the cooling rate depends strongly on the casting speed. Own measurement on samples from a thin strip caster pilot plant, cast at 20 m/min and with a carbon content of 0.06 wt.-% resulted in an austenite grain size of between 400 and 600 µm [28]. For a casting speed of 60 m/min the austenite grain size decreases to 110 µm at the surface and 210 µm in the centre [29].

In welding, the austenite grain size depends strongly on the welding parameters and the heat treatment. Fig. 11 shows the nital etching of a welded joint with clearly visible former austenite grains. This sample has not been reheated and the thermal history is very similar to the aforementioned dipping experiment. The mean austenite grain size (ECD) amounts to 74 µm in correlation with a cooling rate of between 500 and 1000 °C/s [26].

The presented austenite grain size prediction model results in reliable results for all considered technical solidification processes. Uncertainties result from the difficult thermal description of the rapid solidification experiments as well as the regarded processes. The strict validity of the model assumptions for the growth of columnar grains has also to be questioned. The assumption of a linear correlation between carbon content and activation energy is a further simplification: Future work will focus on the influence of other alloying elements on austenite grain growth and hopefully result in a more complex approach.

Fig 11. Nital etching of a welded joint, steel grade in Tab. 2 [26]

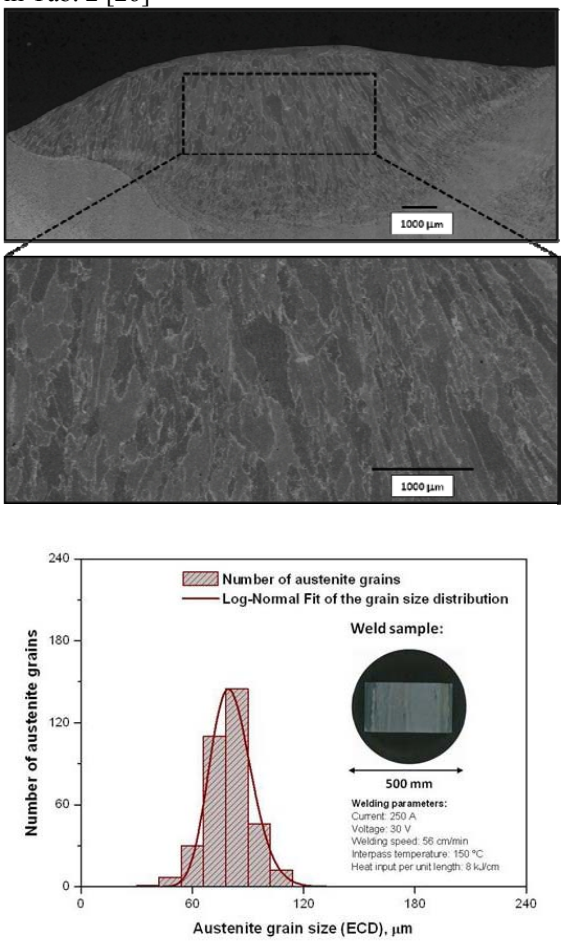

Experiments are a necessity for the adjustment of model parameters. The presented experiments are valuable but, however, have limitations. A very useful direct method, the HT-LSCM, will be described in the next section.

2.1 Direct observation methods – the HT-LSCM method

The high-temperature laser confocal microscopy (HT-LSCM) is today a well established method with growing importance in steel research. The method cannot be described in detail at this point, the authors refer to the voluminous literature [30-34].

HT-LSCM offers the following complementary advantages over the aforementioned experiments:

- HT-LSCM results in a "thermal etching" of the austenite grain boundaries. The grain boundaries become clearly visible for low and lowest carbon steel grades as well as eutectoid steels.

- The results are extremely helpful for the understanding of the nucleation of austenite grains, e.g. during the δ-γ-transformation.
- The direct observation and quantification of the grain growth reduces the number of necessary experiments for the creation of a dataset.

As an example, fig. 12 shows the austenite grain growth for a 0.06 wt.-% C steel (Tab. 3), microalloyed with Nb (0.02 and 0.04 wt.-%). On the left side, for 0.02 wt.-% Nb, the movement of a grain boundary is indicated by the black line. On the right side, the white line highlights two austenite grains. The grains cannot grow due to the pinning forces of non-dissolved Nb(C,N). The dark spots on the sample surface at the right side result from a partial oxidation of the surface.
The subsequent image processing by digital image processing software allows the quantification of the grain size for all time steps. Nevertheless, the samples might also be subjected to metallographic examinations after the experiment. HT-LSCM will be a valuable supplement for the already existing experiments.

Table 3. Steel composition for investigated steel grade in Fig. 12

C, wt.-%	Si, wt.-%	Mn, wt.-%
0,06%	0,2%	0,5%

Fig 12. Austenite grain growth at 1100 °C, steel grades from Tab. 3, microalloyed with 0.02 and 0.04 wt.-% Nb

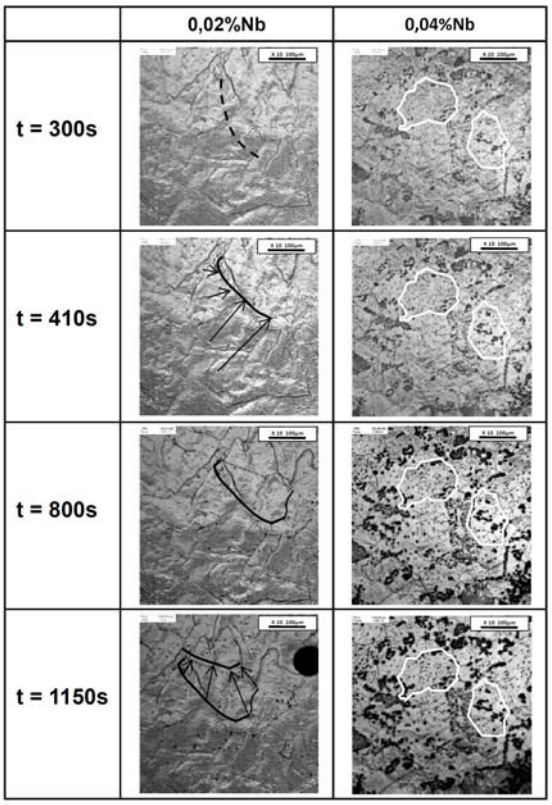

Conclusions

The present paper describes the numerical and physical modelling of austenite grain growth with relevance for technical casting processes.
An already published austenite grain size prediction model was adopted for low carbon content and for higher cooling rates in direct and indirect experiments.
The experimental results serve to adapt the model parameters, the calculation results were verified by grain size measurement on slabs, thin slabs, cast strips and welded joints.
The results point to a sufficient validity of the model over a wide range of cooling conditions and steel compositions.

Acknowledgement

The authors acknowledge the financial support from side of Siemens VAI Metals Technologies and Böhler Welding as well as from the Austrian Research Agency FFG.

References

1. Schwerdtfeger K.: Crack susceptibility of steels in continuous casting and hot forming, Verlag Stahleisen, Duesseldorf, 1994
2. McPherson N.A.; McLean A.: Continuous Casting Vol. 8: Transverse Cracking in Continuously Cast Products, Iron and Steel Society, Warrendale, 1997
3. Mintz B.; Yue S.; Jonas J.J.: Int. Materials Review 36 (1991), 5, pp. 187-217
4. Maehara Y.; Tomono H.; Yasumoto, K.: Trans. ISIJ 27 (1987), pp. 103-109
5. Deprez, P; Bricout J.P. ; Oudin, J.: Mat. Sci. and Engineering, A168 (1993), 17-22
6. Suzuki M.; Hayashi H.; Shibata H.; Emi T.; Lee I.-J.: steel research 70 (1999), 10, pp. 412-419
7. Crowther D.N.; Mintz B.: Mat. Sci. and Technology 2 (1986), pp. 951-955
8. Crowther D.N.; Mintz B.: Mat. Sci. and Technology 2 (1986), pp. 1099-1105
9. Ouchi C.; Matsumoto K.: Trans. ISIJ 22 (1982), pp. 181-189
10. Mintz B.; Crowley A.; Abushosha R.; Crowther D.N.: Mat. Science and Technology 15 (1999), pp. 1179-1185
11. Mintz B.; Abushosha R.; Cowley A.: Mat. Sci. and Technology 14 (1998), pp. 222-226
12. Ohmori Y.; Kunitake T.: Metal Science 17 (1983), pp. 325-332
13. Maehara Y.; Yasumoto K.; Tomono H.; Nagamichi T.; Ohmori Y.: Mat. Sci. and Technology 6 (1990), pp. 793-805

14. Yasumoto K.; Nagamichi T.; Maehara Y.; Gunji K.: Tetsu-to-Hagane (J. Iron Steel Inst. Jpn.) 73 (1987), 14, pp. 1738-1745
15. Bernhard, C.; Reiter, J.; Presslinger, H.: Met. Mat. Trans. B 39 (2008), pp. 885-895
16. Andersen I.; Grong, O.: Acta metal. mater. 43 (1995), 7, pp. 2673-2688
17. Schwerdtfeger K.; Köthe A.; Rodriguez J.M.; W. Bleck: EUR 19409/1 EN, Volume 1, Luxembourg, 2001, pp. 33-48
18. Svoboda, J.; Fischer, F.D.; Fratzl, P.; Kozschnik, E.: Mater.Sci.Eng. A385 (2004), pp. 166-174
19. Kozeschnik, E.; Svoboda, J.; Fratzl, P.; Fischer, F.D.: Mater.Sci.Eng. A385 (2004) pp. 157-165
20. Kikuchi, N.; Nabeshima, S.; Kishimoto, Y.; Ishiguro, Y.; Sridhar, S.: ISIJ International 49 (2009), pp. 1036-1045
21. Reiter, J.; Bernhard, C.; Presslinger, H.: Materials characterization 59 (2008), 6, pp. 737-746
22. Radis, R.; Kozeschnik, E.: Modelling Simul. Mater. Sci. Eng. 18 (2010), pp. 1-8
23. Blejde, W.; Mahapatra, R.; Fukase, H.: Iron- and Steelmaker 27 (2000), No. 4, pp. 29-33
24. Mukunthan, K.; Strezov, L.; Mahapatra, R.; Blejde, W.: Canadian Metallurgical Quarterly 40 (2001), No. 4, pp. 523-532
25. Linzer, B.; Hohenbichler, G.; Bragin, S.; Arth, G.; Bernhard, C.: 3rd International Conference on Simulation and Modelling of Metallurgical Processes in Steelmaking (Steelsim 2009), Leoben, Austria, 8-10 Sept. 2009, Paper - CC17
26. Vanovsek, W; Bernhard, C.; Fiedler, M.; Schnitzer, R.: 65th Annual Assembly and International Conference of the International Institute of Welding, Denver, USA, 8-13th July 2012
27. Bernhard, C.; Guindani, A.; Venturini, R.; Linzer, B.; Jungbauer, A.; Gelder, S.; Bragin, S.: 2nd International Conference on Super High Strength Steels, Peschiera del Garda, Italy, Oct. 2010
28. Bragin, S.: Internal report on metallografic examination on thin slabs, Montanuniversitaet Leoben, 2009
29. Nooning, R.; Killmore, C.R.; Kaul, H.; Phillips, A.; Edelman, D.; Campbel, P.; Williams, J.G.: AISTech 2007, Indianapolis, IN, USA, 7-10 May 2007
30. Sarma, D.S.; Karasev, A.V.; Jönsson, P.G.: ISIJ 49 (2009), pp. 1063-1074
31. Yin, H.; Shibata, H.; Emi, T.; Suzuki, T.: ISIJ Int. 37 (1997), 10, pp. 946-955
32. Shibata H.; Yin, H.; Emi, T.; Yoshinaga, S.: ISIJ Int. 38 (1998), 2, pp. 149-156
33. Reid, M.; Phelan, D.; Dippenaar, R.: ISIJ Int. 44 (2004), 3, pp. 565-572
34. Phelan, D.; Reid, M.; Dippenaar, R.: Comp. Materials Science. 34 (2005), pp. 282-289